Groundwater

Permeability Decline by Clay Fines Migration around a Low-Salinity Fluid Injection Well

by Abdullah Cihan[1,2], Robin Petrusak[3], Pramod Bhuvankar[1], David Alumbaugh[1], Robert Trautz[4], and Jens T. Birkholzer[1]

Abstract

Migration of clay fines can be a concern when less saline fluids are injected into brine-saturated sandstone formations containing clays. If the salinity near fluid injection wells decreases below a critical value, the clay fines near the injection may detach, start migrating, and finally clog the pores. This effect can cause permeability decline near the well and may rapidly reduce the well injectivity. The focus of this work is on evaluating the impacts of clay fines migration on permeability decline in the field, using a numerical model and pressure buildup data collected during successive variable-rate water injections in a deep sandstone reservoir. The numerical model accounts for the mixing of low-salinity water with native brine and the migration of clay fines with the detachment and pore-clogging processes. The model interpretation of the pressure buildup data implies that the observed reduction in well injectivity is mainly associated with the clay fines migration and related pore clogging near the well. The model reasonably well represents the pressure buildup data during the injections. Our simulations demonstrate that the permeability near the well can rapidly decline within the first hour of injection. The measured pressure buildup in post-injection periods appears to decay more rapidly, compared to the simulation results of the model that assume irreversible permeability damage. This raises the question whether the permeability damage may be partly reversible near the well by backflow of brine after the injection of low-salinity water.

Introduction

Migration of fine particles in porous media is of interest to many engineering applications such as water disposal, water treatment, oil recovery, aquifer recharge, geothermal energy, and geological CO_2 storage (Goldenberg et al. 1983; Corapcioglu et al. 1987; Khilar and Fogler 1998; You et al. 2016; Civan 2015; De Silva et al. 2017; Xie et al. 2017). Permeability decline in natural sand layers containing clays can occur when the sand layers initially saturated with high-salinity fluid are exposed to low-salinity water. This phenomenon is referred to as water sensitivity. Depending on the dominant clay minerals present in a natural sand formation, the permeability decline may result from clay detachment and subsequent flow blockage by re-deposition, clay swelling, or a combination of both mechanisms.

Many studies have shown the potential for permeability impairment as a result of water sensitivity in the context of water flooding for oil production or aquifer recharge (e.g., Jones 1964; Brown and Silvey 1977; Goldenberg et al. 1983; Khilar and Fogler 1983; Konikow et al. 2001; Shenglai et al. 2008; Oliveira et al. 2014; Torkzaban et al. 2015). These studies showed that significant decreases in permeability could occur during freshwater injection in unconsolidated and consolidated geologic materials containing a small percentage of dispersible clays such as kaolinite and illite (~5 to 10% by weight). A sharp decrease in permeability was observed after salinity of the injected water dropped below a critical salt concentration (e.g., Khilar and Fogler 1983; Blume et al. 2002). The critical salt concentration was found to be a function of cation type, pH, porous medium properties, and temperature. Similar observations were reported for freshwater flow into brine-bearing sandstones containing significant swelling clays (e.g., smectite), where permeability decline was suggested to occur as a result of migration of swollen fines (Mohan and Fogler 1997; Wilson et al. 2014; Song and Kovscek 2016). The permeability decline by swelling alone reduces the effective area for flow, and

[1]Energy Geosciences Division, Lawrence Berkeley National Laboratory, Berkeley, CA

[2]Corresponding author: Lawrence Berkeley National Lab, Energy Geosciences Division, Earth and Environmental Sciences, 1 Cyclotron Road, Mail Stop 74R316C, Berkeley, CA 94720; acihan@lbl.gov

[3]Advanced Resources International, Inc., Arlington, VA

[4]Electric Power Research Institute, Inc, Palo Alto, CA

Article impact statement: The article shows clay fines detachment causes a rapid decline of near-well permeability and this may be partly reversible by brine backflow.

Received February 2021, accepted August 2021.

doi: 10.1111/gwat.13127

this may be reversible after changing back to the original solution (Mohan et al. 1993; Blume et al. 2002; Fouladi et al. 2021). The non-swelling and swelling clays that detach from pore-grain interface can migrate and accumulate in narrow pore apertures (pore throats) resulting in reduced permeability which some laboratory observations suggest may be permanent (Blume et al. 2002). However, the laboratory studies by Khilar and Fogler (1981, 1983) showed that permeability restoration might be possible by reversing the direction of the flow and flushing the rock with brine after it was exposed to low-salinity water. It was also shown that the detachment of clay fines can be avoided by increasing the salinity of the injected water above the critical salt concentration (e.g., Jones 1964). Clay stabilization approaches such as the use of acidic or alkaline solutions were also reported to prevent the release of the dispersible clays in the field (e.g., Brown and Silvey 1977; Thomas and Crowe 1981; Sloat 1990).

Detachment of clay fines below a critical salinity can be explained conceptually by assessing attractive and repulsive forces between an idealized grain surface and clay particle as a function of salinity. In the presence of high-salinity brine, the clay fines are bound to the grain surfaces by the influences of the Van der Waals (vdW), electric double layer (EDL), and Born-repulsion (BR) forces (Khilar and Fogler 1998; Churaev 2000; Tchistiakov 2000; Israelachvili 2011). The vdW forces act as attractive, and the EDL and BR forces are repulsive. While the actions of the vdW and the EDL forces, depending on electrolyte solution, may extend to a range of up to 100 nm, the BR is a short-range repulsive force that may extend up to several nanometers. The injection of fresh water causes an expansion of the EDL at the grain surface. As the salinity of the mixture decreases, the net force binding the fines to the grain surfaces reduces, and eventually at a critical salinity, the repulsive forces dominate and the fines become free to detach. The size of detached particles has been reported to range from 0.1 to 10 μm (Khilar and Fogler 1998). The injected fresh water exerts hydrodynamic drag and lift forces on the fine particles that can further aid in the removal of the fine particles (Brady et al. 2015; Russell et al. 2017; Chequer and Bedrikovetsky 2019).

Mathematical models developed to describe the permeability decline due to water sensitivity generally assume that fines in porous media can exist in three states: as attached particles, suspended particles, and captured particles. The capture or re-deposition of the fines at pore throats is typically described using a first-order rate equation based on the traditional filtration theory (e.g., Khilar and Fogler 1981; Chequer et al. 2018). Both kinetic and equilibrium-based empirical models were proposed to describe the detachment of fines from grain surfaces. The equilibrium model proposed by Bedrikovetsky et al. (2011) introduces a maximum retention concentration for fines on the grain surfaces as a function of a dimensionless variable representing the ratio between the drag force and the normal force acting on individual fine particles. While this approach to considering microscopic interaction forces is appropriate to pursue in macroscopic model development, application to detachment of multiple clay platelets in large-scale and naturally heterogeneous geologic systems remains a significant challenge (Chequer et al. 2019). The mathematical models based on the first-order capture rate and both types of detachment modeling approaches showed good representation of the permeability decline measured in core-scale experiments. However, limited data exist to test the applicability of the fines migration models to the field scale.

This study focuses on permeability impairment and injectivity reduction as a result of low-salinity fluid injection into a brine-saturated formation. Our focus on injectivity reduction is motivated by a future field demonstration project in Florida under the U.S. Department of Energy's Brine Extraction and Storage Test program, which will evaluate the technical feasibility of managing subsurface pressures associated with large volumes of fluid injection and storage (González-Nicolás et al. 2019). The project plans to inject low-salinity water into isolated layers of brine-saturated Lower Tuscaloosa/Lower Cretaceous sandstone formation for over a year. Thus, understanding the water sensitivity of the injection formation and its potential impact on injectivity is critical. To better understand permeability impairment, we assessed the results of a series of short-term injection tests in an existing well near the injection site. Figure 1 illustrates the unusual increase of injection pressure observed in these tests. The maximum pressure buildup in the well significantly increases from the first test to the second test although the injection rate decreases. The specific injectivity of the well, described as the ratio of the injection rate to the maximum pressure change at the well, consistently decreases from Test 1 to Test 4. As the sand layers into which injection occurred contain significant amounts of clays (10 to 26% by weight), clay particle detachment, migration, and pore clogging could have contributed to the injectivity decline.

In this study, we developed a numerical model and applied it to assess the degree of permeability decline caused by fines migration in the field. The numerical model is based on the conservation of mass equations for water, dissolved salt, and fine particles that include attached fines on the pore-solid interfaces, migrating fines as suspension and captured fines at pore constrictions. The detachment and capture of the fines are described by using first-order nonlinear kinetic equations. The next section of this paper presents a description of the numerical model. We then present model interpretations of the observed pressure changes and numerical simulation results of the permeability impairment by fines migration.

Research Method

Mathematical Model for Coupled Fluid Flow and Fines Migration

To interpret the results of the field data, we use the conservation of mass equations for the aqueous fluid

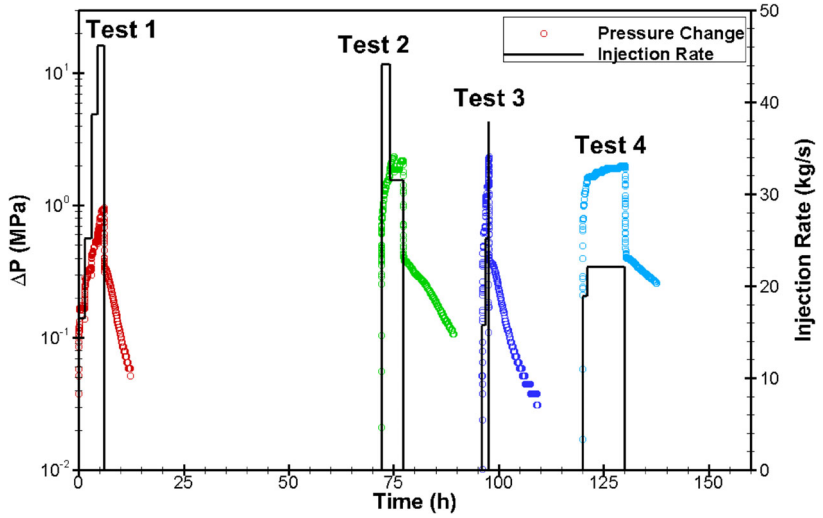

Figure 1. Reservoir pressure increases during successive tests of low-salinity water injection into a brine-saturated geologic formation.

phase, dissolved salt, and the fine particles. We assume the clay fines in sand formations can be present in three states: (1) as particles attached on pore surfaces; (2) as suspended particles in fluid mixture; and (3) as captured particles at pore constrictions. Permeability reduction is caused by the captured particles.

Assuming a binary fluid mixture of water and salt (e.g., NaCl-H_2O), the mass balance equation for a single-phase fluid with variable density and viscosity and the advective-diffusion transport equation for the dissolved salt are expressed as:

$$\frac{\partial(\phi\,\rho)}{\partial t} + \nabla\cdot(\boldsymbol{q}\,\rho) = S \tag{1}$$

$$\frac{\partial(\phi\,w\rho)}{\partial t} + \nabla\cdot(\boldsymbol{q}w\rho - \boldsymbol{D}\phi\cdot\rho\nabla w) = S_w \tag{2}$$

where ρ is the density of the solution (kg/m^3), w is the mass fraction of the dissolved salt in water (−), $\boldsymbol{q}$ is the Darcy velocity (m/s), ϕ is the porosity (−), D is the effective binary diffusion coefficient (m^2/s). S and S_w are the sink/source (production/injection) terms for the aqueous phase and the dissolved salt, respectively. The Darcy velocity vector is expressed as.

$$\boldsymbol{q} = -\frac{\boldsymbol{k}}{\mu}\cdot(\nabla p + \rho g\nabla z) \tag{3}$$

where $\boldsymbol{k}$ is the permeability of the porous medium (a second-order tensor) (m^2) that varies with the captured fine particle concentration as described below, μ is the viscosity of the solution (Pa.s), p is the fluid pressure (Pa), g is the gravitational acceleration (m/s^2) and z is the elevation (m). Density and viscosity of the fluid mixture are functions of salt mass fraction, pressure, and temperature.

The conservation of mass equation for the fines that are released from pore-grain interfaces can be expressed as:

$$\frac{\partial[(1-\phi)\,\sigma_p]}{\partial t} = -r_d \tag{4}$$

where σ_p is the mass of the releasable fines per unit volume of the solid space (kg/m^3) and r_d is the detachment or release rate of the fines (kg/m^3/s). It has been shown both theoretically and experimentally that the clay fines can detach only after salinity decreases below a certain critical salinity in the pore space (e.g., Jones 1964; Khilar and Fogler 1983, 1998; Blume et al. 2002). Recent experimental and pore-scale computational studies (e.g., Chequer et al. 2019; Bhuvankar et al. 2021) suggest that the clay particles detach in large clusters and there exists a critical fluid velocity which needs to be exceeded for the onset of clay detachment. Based on these earlier studies, we express the detachment rate as a function of the critical salinity and the critical velocity as follows:

$$r_d = \alpha\,\Gamma[w_c - w]\Gamma[|\boldsymbol{v}| - v_c]\,\sigma_p(1-\phi) \tag{5}$$

where α is the detachment rate coefficient (m^{-1}) and $\Gamma[\ ]$ is the unit step function that is equal to zero when its argument is less than zero or else is equal to 1. $|\boldsymbol{v}|$ is the magnitude of the mean pore velocity ($\boldsymbol{v} = \boldsymbol{q}/\phi$), v_c is the critical velocity and w_c is the critical salt concentration.

The conservation of mass equation for the suspended fines after their detachment can be expressed as:

$$\frac{\partial(\phi\,c_p)}{\partial t} + \nabla\cdot(\boldsymbol{q}\,c_p - \boldsymbol{D}_p\phi\cdot\nabla c_p) = r_d - r_c \tag{6}$$

where c_p is the mass of the fine particles per unit volume of the pore space (kg/m^3), D_p is the diffusion coefficient for the suspended particles (m^2/s) and r_c is the capture rate of the fines at pore constrictions (kg/m^3/s).

The conservation of mass equation for the fines trapped or captured at pore constrictions can be expressed as:

$$\frac{\partial(\phi\,\sigma_c)}{\partial t} = r_c \tag{7}$$

where σ_c is the mass of the captured fines per unit volume of the pore space (kg/m^3). Based on the classical filtration theory, the capture rate is assumed to be proportional to the flux of the suspended particles as follows:

$$r_c = \beta |\boldsymbol{v}| c_p \phi \tag{8}$$

where β is the capture rate coefficient (m^{-1}). To represent the permeability decline of the porous medium as a function of the captured fines, we employ an empirical permeability equation suggested for sandstones by Khilar and Fogler (1983):

$$k = k_0 \left[1 - \frac{B \phi \sigma_c}{(1-\phi)\sigma_{p0}} \right]^2 \tag{9}$$

where k_0 is the initial intrinsic permeability of the porous medium, σ_{p0} is the initial mass concentration of the releasable fines and B is an empirical constant between 0 and 1.

Numerical Solution Methodology

The coupled non-linear partial differential Equations 1, 2, 4, 6, and 7 are discretized by the Finite Volume Method. We employ a hybrid numerical solution approach that involves sequential solutions of two groups of the equations where the equations in each group are solved in a coupled way. Equations 1 and 2 constitute the first group and Equations 4, 6, and 7 the second group. Iteratively, we solve the first group and then the second group until a global convergence is achieved. The system of equations in each group is linearized using the Newton–Raphson method and solved simultaneously by a preconditioned restarted Generalized Minimum Residual algorithm. At each nonlinear iteration, the solution of the equation system in the first group provides the salinity field and the velocity vector which are used for computation of the equation system in the second group, and then the updated permeability calculated using Equation 9 as a function of the computed captured fines concentration is used in the solution of the first group. The computer code developed for the numerical solution with the migration of fines is built upon an in-house single-phase fluid code with a variable-density and variable-viscosity transport modules (Agartan et al. 2017; Siirila-Woodburn et al. 2017). We utilize the correlations developed by Spivey et al. (2004) and Phillips et al. (1981) to compute the density and the viscosity as a function of salt mass fraction, pressure, and temperature. Dynamic heat flow is not simulated, although the initial formation temperature can vary with depth according to the geothermal gradient.

Model Interpretation of Permeability Decline Using Well Pressure Data

We employed the numerical model described in section Research Methods to interpret the unusual pressure buildup observed during the four successive injection tests at the field site. Only the well head pressure data (at the surface of the injection well) were available. The bottom-hole pressure buildup (i.e., the reservoir pressure buildup at the bottom of the well) was estimated based on the differential changes of the well head pressure with respect to the initial well head pressure before the start of the first injection test. The frictional energy losses through the tubing of the well during injections cause additional pressure drop. After correcting for the frictional losses, the revised values for pressure buildup at the bottom of the well become slightly lower than the values calculated solely from the relative well-head pressure change. All of the results presented in this work, including those in Figure 1, are generated using the corrected pressure buildup data. A detailed description for the estimation of the bottom-hole pressure buildup is provided in Supporting Information (Appendix S1). The data include the pressure recordings of the injection periods and post-injection recovery periods of 6 to 12 h. The data show that the performance of the well, measured by the ratio of the injection rate to the maximum pressure change, declines from one injection to the next.

Reservoir Model

Numerical modeling studies for the injection tests were conducted using a geological model based on data from three wells at the field site. These wells include the existing injection well and two recently drilled wells on the east and north sides of the injection well within 250 and 320 m distances, respectively, from the injection well. Development of the reservoir model relied on the porosity and permeability values obtained from geophysical logs and core materials. An examination of the data for each well indicated that the individual layers of sandstone formation have similar properties, and the estimated permeability values of the model layers in the three well locations are on the same order of magnitude with some minor variability. As a result, we concluded that a "layer-cake" representation of the injection zone based on the geologic characterization data would provide a reasonable model for this analysis.

The geologic model is comprised of 86 layers of poorly consolidated sandstone and claystone of the Lower Tuscaloosa and Lower Cretaceous "Undifferentiated" formations from depths 1450 to 2134 m. Based on sample descriptions and geophysical logs, the contact between the Lower Tuscaloosa and Lower Cretaceous Undifferentiated is estimated to be present at a depth of 1558 m. The geologic model in general contains high-permeability sandstone layers alternating with clay-rich confining layers that are less permeable. In hydrogeological terms, the sandy layers can be characterized as aquifers, and the confining layers as aquitards that have, on average, about two orders of magnitude lower permeability compared to the sandy layers. Porosity, permeability, and thickness of each aquifer and aquitard layer are provided in Supporting Information (Table S1). Figure 2 presents the variations of porosity and permeability with depth. The reservoir

Table 1
Model Input Parameter Values

Initial permeability for aquifers (m^2)	Mean $= 2.51 \times 10^{-12}$ (stdev $= 1.83 \times 10^{-12}$)
Initial permeability for aquitards (m^2)	Mean $= 2.02 \times 10^{-14}$ (stdev $= 1.73 \times 10^{-14}$)
Pore compressibility for aquifers (Pa^{-1})	5.58×10^{-10}
Pore compressibility for aquitards (Pa^{-1})	6.26×10^{-9}
D (m^2/s)	1.00×10^{-10}
D_p (m^2/s)	1.00×10^{-10}
Salinity of the injected fluid (kg/kg)	0.001
Initial salinity of the reservoir fluid (kg/kg)	0.18

Table 2
Whole Rock Mineralogy of the Lower Tuscaloosa Sands at Different Depths

	Mass Percent (%)		
	1496 m	**1550 m**	**1603 m**
Quartz	59.7	62.8	45.2
K-Feldspar	5.5	9.4	9.9
Plagioclase	13.1	16.4	18
Calcite	5	0.5	0
Dolomite	1.1	0.5	0
Pyrite	0.9	0	1
Total non-clay	85.6	89.7	74.1
Total clay	14.4	10.3	25.8
Clay minerals			
Smectite	5.0	2.2	0
Illite/smectite	0.2	2.2	10.9
Illite/mica	4.2	3.7	7.9
Kaolinite	3.1	2.2	4.1
Chlorite	1.9	0	2.9

permeability and compressibility values for the aquifers and the aquitards were calibrated based on fitting of the model without clay fines migration to pressure data from a separate injection test conducted in the field. The test involved injecting brine into one of the newly drilled wells over the entire thickness of the layers and observing the pressure changes in another well. Because there was no previous fresh water injection in this new well, the calibrated reservoir permeability values based on the brine injection test are assumed to represent unperturbed initial permeability $k_0(z)$ in the layer-cake reservoir system. Table 1 lists the input parameters used in the model including the estimated permeability and pore compressibility values.

Table 2 presents X-ray diffraction mineralogy results of representative sidewall cores of sand layers collected near the top of the formation. The results indicate that the cores include a significant amount of both non-swelling clay (kaolinite, illite) and swelling clay (smectite). For the same cores, the clay mineralogy results show that kaolinite constitutes 30 to 65% (by weight) of the $<4\,\mu m$ size clay fraction (not shown in the table). Illite and smectite percentages by weight of the $<4\,\mu m$ size clay fraction range between 3 to 7% and 0 to 18%, respectively. Based on these results, fines migration due to detachment, fines migration due to swelling-induced particle detachment, or a combination of these processes may constitute a risk to well performance.

For representing the injection through a single well in the layered reservoir, we discretized the model in axisymmetric cylindrical coordinates. The model domain extends to 10 km in the radial direction. In the vertical direction, the domain is extended up to a depth of 512 m, representing the thick caprock overlying the Lower Tuscaloosa sands at the field site. Figure 2 shows the structured numerical grid and illustrates the vertical distribution of layer permeability and porosity values. The injection well has 10 cm radius. The well is screened over the entire formation thickness between 1450 and 2134 m. In radial direction, a uniform grid size of 10 cm was selected within 1 m distance near the well and then gradually increases (Figure 2a).

Fixed pressure and fixed concentration boundary conditions were set at the top and lateral boundary of the numerical model domain. No-flow/flux boundary conditions were set at the bottom. Hydrostatic pressure conditions exist before injection starts. The reservoir contains a NaCl dominant water type, with an initial salt mass fraction of 0.18. The temperature at the top of the formation is about 38 °C and assumed to increase linearly with depth based on a geothermal gradient of 0.025 °C/m. The initial values of c_p and σ_c are set to zero. The initial value of the releasable particle concentration, σ_{p0}, is unknown and expected to differ between aquifers and aquitards. A greater decline in permeability occurs as the ratio of σ_c to σ_{p0} and the permeability decay parameter B increase, as represented by the permeability model (Equation 9).

Results

Model Results without Fines Migration

We first used the model to test whether the unusual trend of pressure buildup during the tests can be explained without accounting for clay fines transport. As shown in Figure 3, without the permeability decline (Model w/o fines migration), the maximum pressure buildup would decrease proportional to the injection rates which decrease from the first test to the fourth test. This predicted trend using the model without fines migration is dissimilar to the observed trend of the pressure changes at the well. The predicted pressure changes at very early times of Test 1 are similar to the observed pressure changes, but later the predicted values significantly deviate from the observed data. The model without fines migration significantly underestimates the observed pressure buildup during the

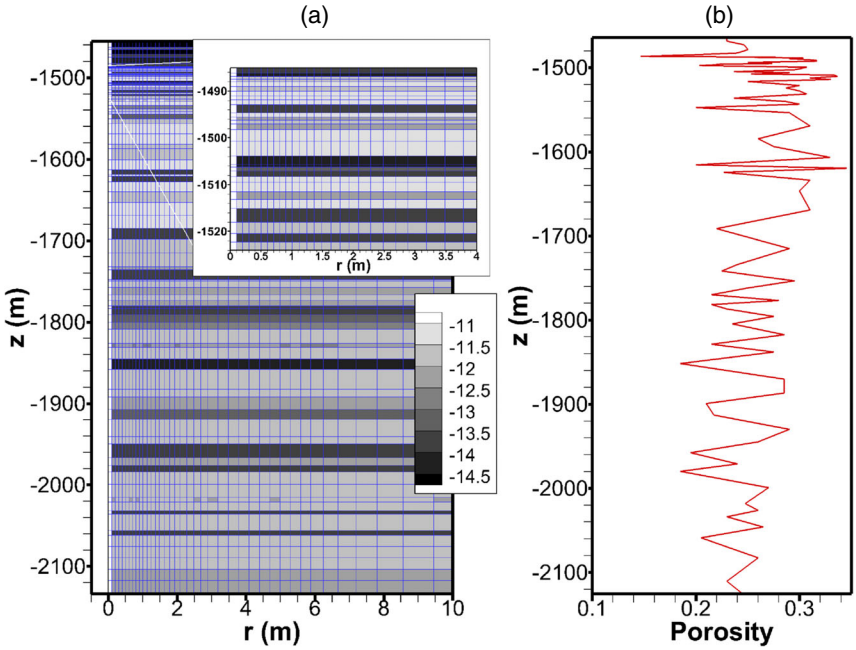

Figure 2. (a) Cross-sectional view of the layer $\log_{10}$ permeability (in m^2) and the model grid used in the reservoir modeling studies. (b) Porosity as a function of depth. The injection well ($r = 0$) with a radius of 10 cm is screened over the entire thickness of the formation. The permeability of the grid cells representing the well is set to 10^{-6} m^2. The grid sizes in the *radial* direction are refined down to 10 cm near the well.

injections. The estimation of the pressure changes without any mechanism of permeability decline clearly contradicts the data.

Model Results and Sensitivity with Fines Migration

The model with fines migration represents reasonably well the overall pressure buildup during injection periods (Model w/fines migration, Figure 3). The simulated pressure buildup during the recovery periods (post-injection) decreases at a slower rate than the data, especially for Tests 3 to 4. Potential reasons for the overestimation of the pressure increases in post-injection periods are explained in the Discussion section. Table 3 lists the estimated 12 parameters that include six model parameters (α, w_c, β, B, σ_{p0}, and v_c) separately defined for aquifers and aquitards. The unknown parameters were estimated using the Differential Evolution (DE) optimization algorithm (Price et al. 2005). The DE, a derivative-free global optimization algorithm, has been successfully used to find optimal solutions that involve a large number of unknown parameters in our earlier studies (e.g., Cihan et al. 2015, 2017) as in this study.

Detachment rate coefficient (α), critical salinity (w_c), and critical velocity (v_c) parameters characterize the detachment rate of the clay fines. The estimated lower detachment rate and higher critical velocity (α_{aqt} and $v_{c,aqt}$) in Table 3 for the aquitard layers indicate that the mobilization of clay fines through aquitards require a stronger hydrodynamic force, represented by a higher critical velocity in the model, and that detachment occurs more slowly compared to the detachment in the aquifers. The estimated value of the critical salt mass fraction for the aquifer layers ($w_{c,aq} = 0.004$) is very similar to the reported values for NaCl-saturated sandstones containing dispersible clays such as kaolinite and illite (Khilar and Fogler 1998). The critical salt mass fraction can be as large as 0.015 for some other NaCl-saturated sandstones containing significantly more swelling clays (smectite) than dispersible clays (Mohan and Fogler 1997). The critical mass fraction for aquitards ($w_{c,aqt}$) was estimated to be about 0.009. The estimated $w_{c,aqt}$ falling between these reported values (of 0.004 and 0.015) might indicate that both the dispersible and the swelling-induced fines migration can result in permeability reduction in the aquitards. The permeability decay parameter (B) and the capture rate coefficient (β) in the aquifers were estimated to be significantly greater than in the aquitards. The greater values of B_{aq} and β_{aq} indicate that the permeability reduction is expected to be more severe in the aquifers.

We conducted a local sensitivity analysis to obtain insights on the effects of parameter uncertainty on the model results for pressure increases. Normalized sensitivity coefficients were calculated based on evaluating the partial derivative of the residual pressure change with respect to each selected parameter as $p_{\text{ibest}}/U_{best}(t_N)\,\partial U(t_N)/\partial p_i$, where U is defined as a summation of the calculated pressure changes with respect to the observed pressure changes: $\sum_{i=1}^{N} |\Delta P_{cal}(t_i) - \Delta P_{obs}(t_i)|$, where N is the total number of the cumulative pressure measurements by the end of each test periods including the post-injection periods of the tests. p_{i} is the ith parameter value, and subscript *best* indicates the optimal or base parameter values. The tabulated sensitivity values and

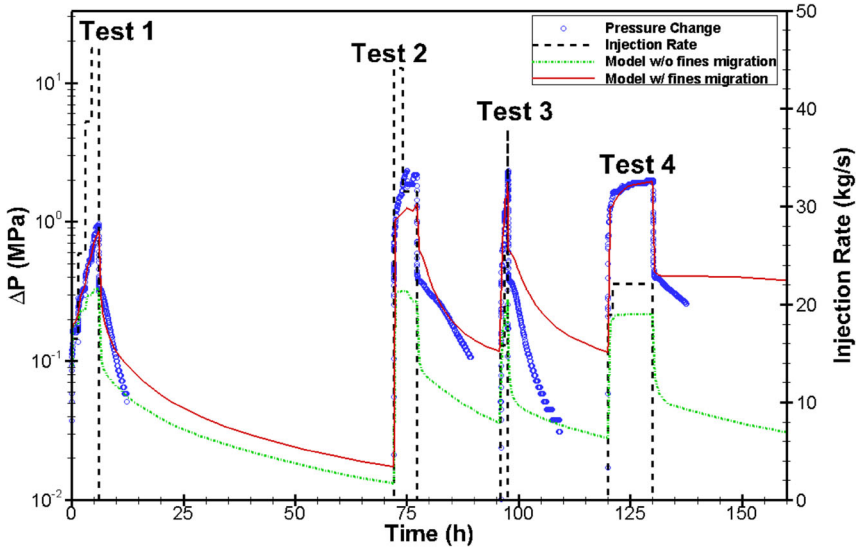

Figure 3. Comparisons of the numerical model results with the pressure buildup data at the well with and without the fines migration processes and permeability decline in the models. The model with fine migration was attempted to fit the entire data set during all the injection tests.

Table 3
Estimated Parameter Values and Sensitivity of the Model Output to Variation in Each Parameter

		Sensitivity							
	Best Estimate	**Test 1**		**Tests 1, 2**		**Tests 1, 2, 3**		**Tests 1, 2, 3, 4**	
α_{aq}	2.337×10^{-4}	1.36	2	8.50×10^{-1}	2	8.20×10^{-1}	3	1.78×10^{-1}	3
β_{aq}	7.787×10^{3}	1.49×10^{-2}	4	3.71×10^{-2}	4	5.92×10^{-2}	5	1.12×10^{-2}	8
$w_{c,aq}$	0.004	6.78×10^{-2}	3	1.67×10^{-1}	3	1.52×10^{-1}	4	7.23×10^{-2}	4
B_{aq}	0.957	5.00	1	7.60	1	1.56×10^{1}	1	2.31×10^{1}	1
$\sigma_{p0,aq}$	4.635	3.94×10^{-4}	7	6.37×10^{-3}	8	4.03×10^{-3}	11	2.77×10^{-2}	7
$v_{c,aq}$	1.649×10^{-6}	9.52×10^{-5}	12	6.77×10^{-5}	12	2.78×10^{-2}	8	1.11×10^{-2}	9
α_{aqt}	1.518×10^{-5}	2.44×10^{-4}	11	7.23×10^{-3}	6	1.39×10^{-2}	10	5.48×10^{-2}	5
β_{aqt}	89.510	3.72×10^{-4}	8	4.72×10^{-3}	9	1.81×10^{-2}	9	1.11×10^{-2}	10
$w_{c,aqt}$	0.009	3.26×10^{-4}	9	7.22×10^{-3}	7	5.83×10^{-2}	6	4.15×10^{-3}	11
B_{aqt}	0.737	3.05×10^{-4}	10	1.96×10^{-2}	5	5.39×10^{-2}	7	3.30×10^{-2}	6
$\sigma_{p0,aqt}$	10.843	3.95×10^{-4}	6	3.11×10^{-3}	10	2.89×10^{-5}	12	3.25×10^{-3}	12
$v_{c,aqt}$	2.565×10^{-6}	4.12×10^{-4}	5	2.45×10^{-3}	11	1.53	2	2.11	2

Notes: α is the detachment rate coefficient (s^{-1}), β is the capture rate coefficient (m^{-1}), w_c is the critical salinity (−), B is the permeability decay parameter (−), σ_{p0} is the releasable clay concentration (kg/m^3), and v_c is the critical velocity (m/s). Subscripts *aq* and *aqt* refer to the parameters for aquifers and aquitards, respectively.

the integer numbers next to them listed in each column of Table 3 represent the contribution of each parameter to the model output, relative to the contributions of the other parameters. The sensitivity values are presented for each of the cumulative time periods that consist of Test 1, Test 1 + 2, Test 1 + 2 + 3 and Test 1 + 2 + 3 + 4. Higher sensitivity values and lower integer numbers for a parameter indicate that its estimation from the pressure data is more reliable, compared to the less sensitive parameters with higher integer numbers listed in the same column.

The most sensitive parameter during all the injection periods appears to be the permeability decay parameter, B_{aq}, for aquifers. Very small changes in the permeability decay parameter, B_{aq}, around its best-fit value lead to significant changes in the pressure buildup values. B controls the final possible value of the reduced permeability after all the releasable clays detach and become captured. The finding that the model results are very sensitivity to the B_{aq} value of the aquifers shows the importance of correctly describing the relationship between the permeability and the concentrations of the releasable and captured clay fines for accurate prediction of the pressure buildup. The model results for the pressure buildup seem to be much less sensitivite to the permeability decay parameter, B_{aqt}, for aquitards. The lower sensitivity value does not necessarily mean that B_{aqt} is an unimportant parameter, because B directly affects the reduced permeability of the aquitards and thus the pressure dissipation across the domain around the well. In general, the lower sensitivity values calculated for the

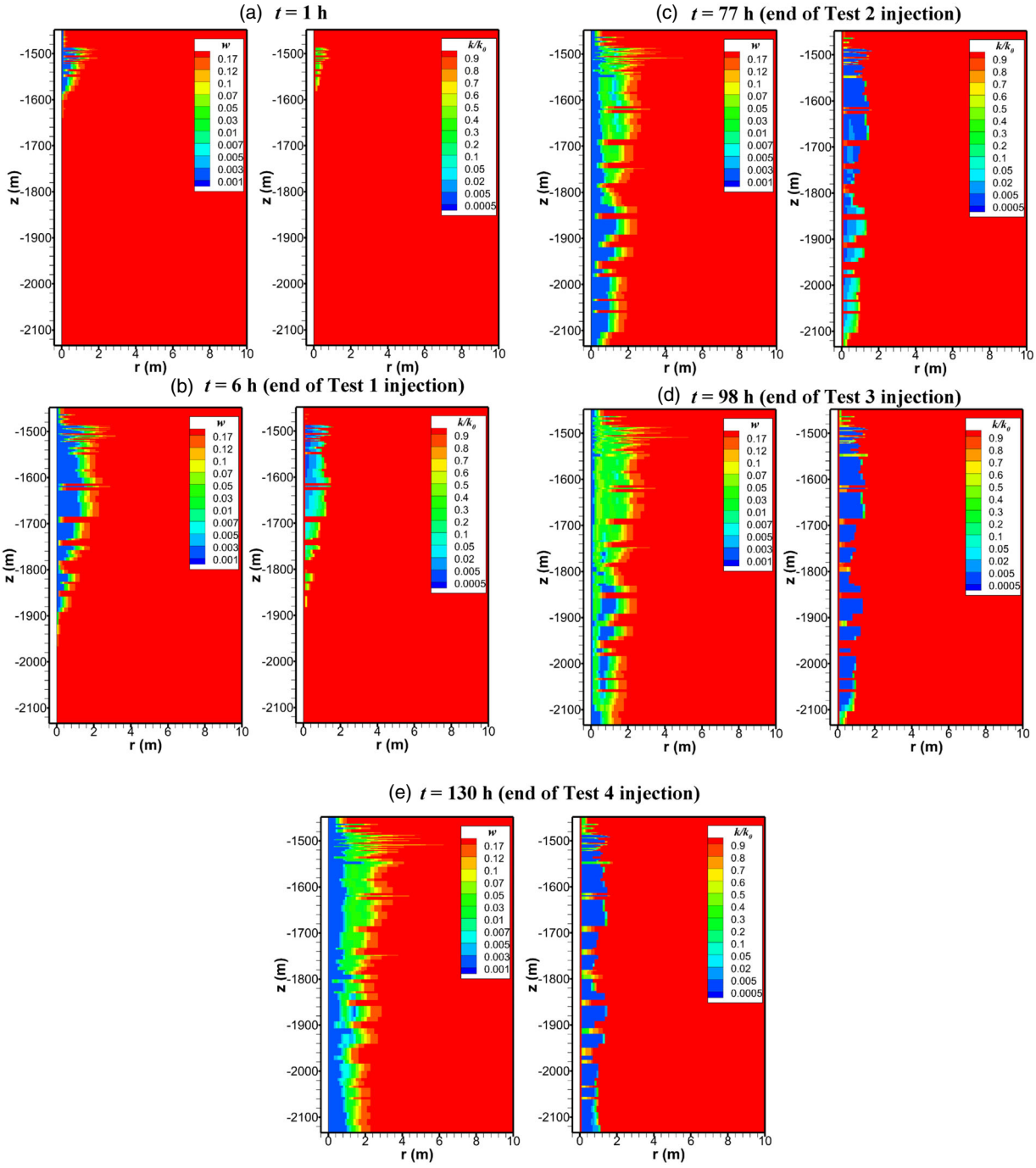

Figure 4. Changes in salinity (left) and permeability (right) near the well. (a) The first hour of Test 1 injection, (b) 6 h, end of the injection for Test 1, (c) 77 h (end of Test 2 injection), (d) 98 h (end of Test 3 injection), and (e) 130 h (end of Test 4 injection).

aquitard parameters reflect the fact that the permeability of the aquitards appears much less impacted within the time frame of the injections, compared to the permeability of the aquifers.

Figure 4 presents the spatial extent of salinity changes and permeability decline around the well, simulated by the model at an early time and at the end time of the injection tests. Figure 4a (right) shows that the permeability of the top aquifer layers rapidly declines within the first hour of Test 1. As the permeability of the aquifer layers near the top diminishes after the first injection test (Figure 4a and 4b), the lighter freshwater progressively invades deeper aquifer layers during the second injection test (Figure 4c). However, a noticeable freshwater invasion into the aquitard layers does not occur until the third and the fourth injections (Figure 4c and 4d). With more freshwater entry into the aquitard layers, the model results start to show more sensitivity to some of the model parameters for the aquitards (Table 3). $v_{c,\mathrm{aqt}}$ becomes the second most sensitive model parameter when considering the entire

data collected by the third and the fourth injection tests. At the end of the fourth injection, the permeability of the layers near the well is impacted along the entire thickness, albeit more severe for the aquifer layers (Figure 4e).

In between the injections (Tests 1 to 2, Tests 2 to 3, and Tests 3 to 4), the mixing of the freshwater and brine is controlled by diffusion, natural convection, and vertical permeability variation. These mixing processes create highly heterogeneous initial conditions of salinity for Tests 2, 3, and 4 injections. As a result of the heterogeneous initial salinity, the interface between the low-salinity water and brine becomes very diffuse during Tests 2, 3, and 4 injections (Figure 4c through 4e, left). At the end of Test 4 injection, the permeability damage zone around the well extends to about 1.5 m radial distance, as can be seen from Figure 4e, right. However, most of the aquifer permeability damage develops during the first two tests. The minimal advancement of the permeability damage zone in the aquifer layers during Tests 3 and 4 is caused by the significant reduction of permeability that slows down the radial movement of the low-salinity water front ($<w_{c,aq}$). The slow down of the damage at later times causes small reductions in the relative sensitivities calculated for the aquifer layer parameters such as α_{aq}, $w_{c,aq}$, and β_{aq}, when including the data from Tests 3 and 4.

Discussion

The recorded falloff of pressure buildup in between injections, especially for Tests 3 and Test 4, occurs more rapidly, compared to the numerical model results (Figure 3). The model includes an assumption of irreversible permeability damage once it occurs. The rapid decay of the pressure buildup raises the question whether the permeability damage at the field may be partly reversible after the injection stops. The mineralogical analyses using a limited number of cores from the sandstone formation at the field show that the formation layers include significant amount of both non-swelling clay (kaolinite, illite) and swelling clay (smectite). As a result, freshwater flow into the brine-bearing Lower Tuscaloosa sandstones may cause the permeability to decline due to the migration of both non-swelling and swollen fines. The swelling alone, in addition to the migration of fines, might be more likely to occur in the aquitard layers, and the permeability decline by swelling alone may be reversible after changing back to the original brine solution (Mohan et al. 1993; Blume et al. 2002). Some laboratory studies suggest that the permeability decline due to the clay fines migration may be permanent (e.g., Blume et al. 2002). However, the core-scale experimental investigations by Khilar and Fogler (1981, 1983) showed that permeability might be restored by flushing the rock with brine in the opposite direction after the rock was exposed to low-salinity water.

Although the model used in this study does not include any mechanism of reversible permeability damage, we demonstrate in Figure 5 that a similar flow reversal to the Khilar and Fogler's experimental condition at the laboratory can occur at the field after stopping the injection. After the injection stops, the lighter fluid invading the lower layers of the formation tends to flow upward due to buoyancy. The upward buoyant flow of lighter

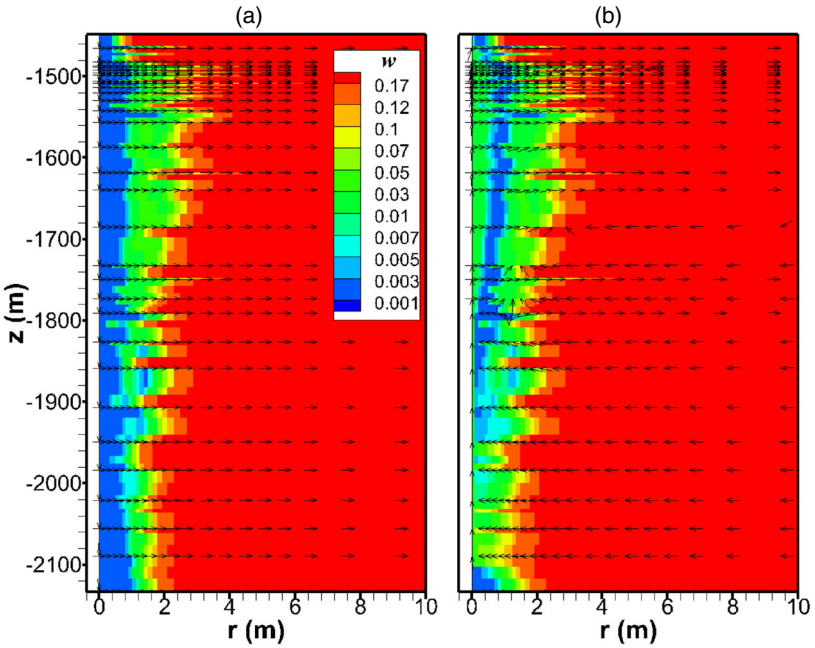

Figure 5. Demonstration of flow reversal and salinity changes after Test 4 injection. (a) Right before stopping the injection. (b) 36 h after Test 4 injection. The arrows show that in the post-injection period, the velocity vectors near the well change from radially outward direction to inward direction in all the layers below a depth of about 1830 m and in some intermediate layers above it.

fluid preferentially occurs through the lowest resistance path, that is, through the well. As a result, as shown in Figure 5b, the low-salinity fluid in some formation layers near the well is displaced by the backflow of brine toward the well. The hypothesis for the permeability restoration is as follows: With the backflow of brine, some of the clay particles can dislodge from the pore throats and attach back to pore body-grain surfaces due to the increased attractive forces with increasing salinity, which result in increase of the permeability. Testing of this hypothesis requires detailed pore-scale experimental and computational studies, which are currently very limited. Such advanced studies would help better understanding the mechanisms of clay fines migrations and developing more accurate macroscopic models to be used at field scale such as presented in this paper.

The reduction in injectivity at the site as a result of low-salinity water injection constitutes a risk for the future field demonstration project in Florida, as stated in Introduction. The field demonstration project involves injection of low-salinity water from a new injection well into two layers at about 1500 m depth in the Tuscaloosa Massive sand, at an average rate of $\sim$545 m^3/d. For this planned injection rate, the model results show that the impacts of the permeability impairment may appear within several hours to a few days of the injection. The common approach to dissolve the pore-clogging fines in the field is to apply acid treatment. As an alternative, based on the hypothesis of the permeability restoration above, hydraulic control-based field methods (e.g., injection/extraction) may be tested to direct brine flow toward the well of which injectivity is significantly reduced for the purpose of remediation. However, a more plausible approach for the successful completion of the field demonstration project should be to prevent the loss of injectivity by chemical control of the injected water. The modeling analysis suggests that the detachment of clay fines can be avoided by increasing the salinity of the injected water above the critical salt concentration ($\sim$4000 to 9000 ppm).

Another important point that deserves to be discussed is the data availability for this type of field-scale research study. The model sensitivity analyses show the importance of the successive injection tests with variable rates for both diagnosing the permeability impairment in sandstones containing clays and characterizing the fines migration model parameters. In addition to the pressure measurements, as used in this work, well log or geophysical measurements might be useful for testing the model predictions and better understanding the degree of permeability impairment. However, nuclear magnetic resonance logging tools that are used to measure permeability, cannot detect permeability damage that extends 0.5 to 1 m away from the wellbore, as the model results suggest. Resistivity logs based on the 3D resistivity imaging as reported by Wilson et al. (2019) may sense the permeability changes near the well, although the resistivity changes caused by the fines migration would likely be negligible compared to those changes caused by the mixing of brine with low-salinity water. High frequency seismic and sonic methods may be used as a possible geophysical technique to image subtle velocity changes in the formation due to fines migration. Common sonic well logging tools often lack the energy to image more than a 0.3 to 0.6 m away from the borehole. Installing a permanent crosswell seismic monitoring system such as that reported in Daley et al. (2007) and Silver et al. (2007) might provide the necessary resolution if the two wells are close enough together, but it is unlikely that the movements of the fines would cause a large enough velocity change to be detectable. In addition, the successful implementation of this method requires that the formation is well-cemented and consolidated such that no significant sand particle displacements other than clay fines occur. Otherwise, significant changes in the sand formation matrix due to the injection process surrounding the borehole can produce velocity changes that are greater than those caused by the fines migration. Using the existing methods, it seems currently challenging to accurately visualize the changes associated with the migration of clay particles in poorly consolidated formations.

Conclusions

A numerical model has been applied to investigate the contribution of clay fines release and migration to the apparent decline in permeability and injectivity observed at a field site during a series of four injection tests of fresh water into a brine aquifer. The brine-saturated reservoir system contains 10 to 26% clay, with the dominant clay minerals kaolinite, smectite, and illite. The numerical model that simulates the mixing of the low-salinity water with brine and the migration of clay fines with detachment and capture mechanisms represents the increase of pressure reasonably well during the injection periods. The findings imply that the reduction in permeability or injectivity at the site is mainly associated with the migration of clay fines. Our simulations show that the permeability of the aquifer layers near the top Lower Tuscalossa sandstones rapidly declines within the first hour of Test 1. At the end of the fourth injection, the permeability of both aquifer and aquitard layers near the well is impacted along the entire thickness, but the reduction in the aquifer permeability is estimated to be much more significant. The model shows that the permeability damage zone around the well extends to about 1.5 m radial distance. The model analyses indicate the importance of the multiple injection tests with variable rates for both diagnosing the permeability impairment in sandstone aquifers and characterizing the fines migration model parameters.

The observed pressure buildup in post-injection periods appears to decay more rapidly, compared to the model-estimated pressure buildup. The model assumes that the permeability damage is irreversible once it develops. The rapid decay of the pressure buildup after the low-salinity water injections indicates that the permeability damage may be partly reversible by the backflow

of brine toward the well. The results point to the need for better understanding the mechanisms of clay fines migration, swelling, and reversible permeability damage through advanced experimental and computational studies. Our study also points to the need for improved monitoring approaches near the wells to visualize the changes associated with the migration of clay particles.

Acknowledgments

This material is based upon work supported by the Department of Energy under Award Number DE-FE0026140. The authors would like to thank Southern Company Services Research & Development in Birmingham, Alabama, Gulf Power Company, in Pensacola, Florida, and Jacobs Engineering for sharing existing field data and advice used in the preparation of this work. The authors would also like to thank to two anonymous reviewers for their constructive comments.

Disclaimer

This report was prepared as an account of work sponsored by an agency of the U.S. Government. Neither the U.S. Government nor any agency thereof, nor any of their employees, makes any warranty, express or implied, or assumes any legal liability or responsibility for the accuracy, completeness, or usefulness of any information, apparatus, product, or process disclosed, or represents that its use would not infringe privately owned rights. Reference herein to any specific commercial product, process, or service by trade name, trademark, manufacturer, or otherwise does not necessarily constitute or imply its endorsement, recommendation, or favoring by the U.S. Government or any agency thereof. The views and opinions of authors expressed herein do not necessarily state or reflect those of the U.S. Government or any agency thereof.

Authors' Note

The authors do not have any conflicts of interest or financial disclosures to report.

Supporting Information

Additional supporting information may be found online in the Supporting Information section at the end of the article. Supporting Information is generally *not* peer reviewed.

Appendix S1. Estimation of the bottom-hole pressure.
Table S1. Porosity, permeability, and thickness of each aquifer and aquitard layer.

References

Agartan, E., A. Cihan, T.H. Illangasekare, Q. Zhou, and J.T. Birkholzer. 2017. Mixing and trapping of dissolved CO_2 in deep geologic formations with shale layers. *Advances in Water Resources* 105: 67–81.

Bedrikovetsky, P., F.D. Siqueira, C.A. Furtado, and A.L.S. Souza. 2011. Modified particle detachment model for colloidal transport in porous media. *Transport in Porous Media* 86, no. 2: 353–383.

Bhuvankar, P., A. Cihan, and J.T. Birkholzer. 2021. Pore-scale CFD simulations of clay mobilization in natural porous media due to fresh water injection. *Chemical Engineering Science*, in press.

Blume, T., N. Weisbrod, and J.S. Selker. 2002. Permeability changes in layered sediments: Impact of particle release. *Ground Water* 40, no. 5: 466–474.

Brady, P.V., N.R. Morrow, A. Fogden, V. Deniz, and N. Loahardjo. 2015. Electrostatics and the low salinity effect in sandstone reservoirs. *Energy & Fuels* 29, no. 2: 666–677.

Brown, D. L., and W. D. Silvey. 1977. Artificial recharge to a freshwater-sensitive brackish-water sand aquifer, Norfolk, Virginia. U.S. Geol. Survey Prof. Paper 939, 53.

Chequer, L., and P. Bedrikovetsky. 2019. Suspension-colloidal flow accompanied by detachment of oversaturated and undersaturated fines in porous media. *Chemical Engineering Science* 198: 16–32.

Chequer, L., P. Bedrikovetsky, T. Carageorgos, A. Badalyan, and V. Gitis. 2019. Mobilization of attached clustered colloids in porous media. *Water Resources Research* 55: 5696–5714.

Chequer, L., A. Vaz, and P. Bedrikovetsky. 2018. Injectivity decline during low-salinity waterflooding due to fines migration. *Journal of Petroleum Science and Engineering* 165: 1054–1072.

Churaev, N.V. 2000. *Liquid and Vapor Flows in Porous Bodies: Surface Phenomena*. New York: CRC Press.

Cihan, A., J.T. Birkholzer, L. Trevisan, A. Gonzalez-Nicolas, and T.H. Illangasekare. 2017. Investigation of representing hysteresis in macroscopic models of two-phase flow in porous media using intermediate scale experimental data. *Water Resources Research* 53: 199–221.

Cihan, A., J.T. Birkholzer, and M. Bianchi. 2015. Optimal well placement and brine extraction for pressure management during CO_2 sequestration. *International Journal of Greenhouse Gas Control* 42: 175–187.

Civan, F. 2015. *Reservoir Formation Damage*. Elsevier Inc., Oxford, UK.

Corapcioglu, Y.M., N.M. Abboud, and A. Haridas. 1987. Governing Equations for Particle Transport in Porous Media. In *Advances in Transport Phenomena in Porous Media*. Dordrecht: Martinus Nijhoff Publishers.

Daley, T.M., R.D. Solbau, J.B. Ajo-Franklin, and S.M. Benson. 2007. Continuous active-source seismic monitoring of CO2 injection in a brine aquifer. *Geophysics* 72: A57–A61.

De Silva, G.P.D., P.G. Ranjith, M.S.A. Perera, Z.X. Dai, and S.Q. Yang. 2017. An experimental evaluation of unique CO_2 flow behavior in loosely held fine particles rich sandstone under deep reservoir conditions and influencing factors. *Energy* 119: 121–137.

Fouladi, M.M., K. Hassani, B. Rostami, and P. Pourafshary. 2021. Experimental studies of low salinity water flooding in sandstone porous media: Effects of the presence of silica and kaolinite. *Energy Sources, Part A: Recovery, Utilization, and Environmental Effects*. https://doi.org/10.1080/15567036.2020.1859019

Goldenberg, L.C., M. Magaritz, and S. Mandel. 1983. Experimental investigation on irreversible changes of hydraulic conductivity on the seawater-freshwater interface in coastal aquifers. *Water Resources Research* 19, no. 1: 77–85. https://doi.org/10.1029/WR019i001p00077

González-Nicolás, A., A. Cihan, R. Petrusak, Q. Zhou, R. Trautz, D. Riestenberg, M. Godec, and J.T. Birkholzer. 2019. Pressure management via brine extraction in geological CO_2 storage: Adaptive optimization strategies under poorly characterized reservoir conditions. *International Journal of Greenhouse Gas Control* 83: 176–185.

Israelachvili, J.N. 2011. *Intermolecular and Surface Forces*, 3rd ed. Elsevier, Oxford, UK.

Jones, F.O. 1964. Influence of chemical composition of water on clay blocking of permeability. *Journal of Petroleum Technology* 16: 441–446.

Khilar, K.C., and H.S. Fogler. 1998. *Migrations of Fines in Porous Media*. Dordrecht: Kluwer Academic Publishers.

Khilar, K.C., and H.S. Fogler. 1983. Water sensitivity of sandstones. *Society of Petroleum Engineers Journal* 23: 55–64.

Khilar, K.C., and H.S. Fogler. 1981. *Surface Phenomena in Enhanced Oil Recovery*. New York: Plenum Publishing Corp.

Konikow, L.F., L.L. August, and C.I. Voss. 2001. Effects of clay dispersion on aquifer storage and recovery in coastal aquifers. *Transport in Porous Media* 43: 45–64.

Mohan, K.K., and H.S. Fogler. 1997. Colloidally induced smectitic fines migration: Existence of microquakes. *AICHE Journal* 43, no. 3: 565–576.

Mohan, K.K., R.N. Vaidya, M.G. Reed, and H.S. Fogler. 1993. Water sensitivity of sandstones containing swelling and non-swelling clays. *Colloids and Surfaces A: Physicochemical and Engineering Aspects* 73: 237–254.

Oliveira, M.A., A.S.L. Vaz, F.D. Siqueira, Y. Yang, Z. You, and P. Bedrikovetsky. 2014. Slow migration of mobilised fines during flow in reservoir rocks: Laboratory study. *Journal of Petroleum Science and Engineering* 122: 534–541.

Phillips, S.L., A. Igbene, J. A. Fair, H. Ozbek, and M. Tavana. 1981. A technical databook for geothermal energy utilization. Lawrence Berkeley National Laboratory Report LBL-12810, Berkeley, California.

Price, K., R. Storn, and J. Lampinen. 2005. *2005. Differential Evolution: A Practical Approach to Global Optimization*. Berlin, Germany: Springer.

Russell, T., D. Pham, M.T. Neishaboor, A. Badalyan, A. Behr, L. Genolet, P. Kowollik, A. Zeinijahromi, and P. Bedrikovetsky. 2017. Effects of kaolinite in rocks on fines migration. *Journal of Natural Gas Science and Engineering* 45: 243–255.

Shenglai, Y., S. Zhichao, L. Wenhui, S. Zhixue, W. Ming, and Z. Jianwei. 2008. Evaluation and prevention of formation damage in offshore sandstone reservoirs in China. *Petroleum Science* 5: 340–347.

Siirila-Woodburn, E.R., A. Cihan, and J.T. Birkholzer. 2017. A risk map methodology to assess the spatial and temporal distribution of leakage into groundwater from Geologic Carbon Storage. *International Journal of Greenhouse Gas Control* 59: 99–109.

Silver, P.G., T.M. Daley, F.L. Niu, and E.L. Majer. 2007. Active sourve monitoring of cross-well seismic travel time for stress-induced changes. *Bulletin of the Seismological Society of America* 97: 281–293.

Sloat, B.F. 1990. Field test results with alkaline potassium solutions to stabilize clays permanently. *SPE Reservoir Engineering* 5: 143–146.

Song, W., and A.R. Kovscek. 2016. Direct visualization of pore-scale fines migration and formation damage during low-salinity water flooding. *Journal of Natural Gas Science and Engineering* 34: 1276–1283.

Spivey, J.P., W.D. Mccain, and R. North. 2004. Estimating density, formation volume factor, compressibility, methane solubility, and viscosity for oilfield brines at temperatures from 0 to 275°C, pressures to 200 MPa, and salinities to 5.7 mole/kg. *Journal of Canadian Petroleum Technology* 43: 7.

Tchistiakov, A.A. 2000. Colloid chemistry of in situ clay-induced formation damage. *Society of Petroleum Engineers* 58747: 1–9.

Thomas, R.L., and C.W. Crowe. 1981. Matrix treatment employs new acid system for stimulation and control of fines migration in sandstone formations. *Journal of Petroleum Technology* 33: 1491–1500.

Torkzaban, S., S.A. Bradford, J.L. Vanderzalm, B.M. Patterson, B. Harris, and H. Prommer. 2015. Colloid release and clogging in porous media: Effects of solution ionic strength and flow velocity. *Journal of Contaminant Hydrology* 181: 161–171.

Wilson, G., D. Marchant, E. Haber, N. Clegg, D. Zurcher, L. Rawshorne, and J. Kunnas. 2019. Real-time 3D inversion of ultra-deep resistivity logging-while-drilling data. Presented at the Society of Petroleum Engineers Annual Technical Conference and Exhibition. Paper SPE-196141-MS.

Wilson, M.J., L. Wilson, and I. Patey. 2014. The influence of individual clay minerals on formation damage of reservoir sandstones: A critical review with some new insights. *Clay Minerals* 49: 147–164.

Xie, Q., A. Saeedi, C.D. Piane, L. Esteban, and P.V. Brady. 2017. Fines migration during CO_2 injection: Experimental results interpreted using surface forces. *International Journal of Greenhouse Gas Control* 65: 32–39.

You, Z., Y. Yang, A. Badalyan, P. Bedrikovetsky, and M. Hand. 2016. Mathematical modelling of fines migration in geothermal reservoirs. *Geothermics* 59: 123–133.